Journal of Physics and Chemistry of Solids 212 (2026) 113519

Contents lists available at ScienceDirect

Journal of Physics and Chemistry of Solids

journal homepage: www.elsevier.com/locate/jpcs

Thermoluminescence, electron paramagnetic resonance, and structural characterization of natural prehnite for high-dose radiation dosimetry

Monise B. Gomes [a,*], Carlos D. Gonzales-Lorenzo [b,c,**], René R. Rocca [d,***], F.N. Ramirez [e,f,****], Edy E. Cuevas-Arizaca [g], Betzabel N. Silva-Carrera [b], T.K. Gundu Rao [c], Nilo F. Cano [d], Jose F.D. Chubaci [a,b,*****]

[a] Instituto de Pesquisas Energéticas e Nucleares, IPEN-CNEN/SP, São Paulo, SP, Brazil
[b] Instituto de Física, Universidade de São Paulo, São Paulo, SP, Brazil
[c] Universidad Nacional de San Agustín de Arequipa, Av. Independencia S/N, Arequipa, Peru
[d] Instituto do Mar, Universidade Federal de São Paulo, Santos, SP, Brazil
[e] Universidad Nacional de Piura UNP, Miraflores S/N, Piura, Peru
[f] Universidad Católica Sapientae UCSS, Piura, Peru
[g] Vicerrectorado de Investigacion, Universidad Catolica de Santa Maria, Arequipa, Peru

ARTICLE INFO

Keywords:
Prehnite
Gamma radiation
Rietveld refinement
TL
EPR
XRF

ABSTRACT

Natural prehnite was evaluated as a thermoluminescence (TL) material for high-dose dosimetry. XRF identified SiO_2, Al_2O_3, and CaO as major constituents. Prehnite samples annealed between 200 and 800 °C (1 h) were examined by XRD and Rietveld analysis, confirming prehnite as the majority phase and revealing calcite and vaterite after heating. The 600 °C sample provided the highest TL yield and was selected for detailed study. Fading tests showed a ~40 % loss in the 240/350 °C peaks over 5.42 days (130 h), followed by signal stability. Dose–response demonstrated, for the 245 peak and 325 °C, a linear region in the 0.1–2 kGy and 0.5–20 kGy range, respectively, with saturation occurring between 30 and 100 kGy. Kinetic parameters were obtained using TM-Tstop, initial-rise, and variable-heating-rate methods; glow-curve deconvolution resolved five TL components. TL spectra display an intense band near 530 nm and a weak 550 nm band, suggesting two main recombination centers.

1. Introduction

The development of thermoluminescent (TL) materials for radiation dosimetry is essential for applications in medical, industrial, and environmental monitoring, as well as in extreme radiation environments such as space exploration and nuclear accident scenarios. Silicate-based minerals, including feldspar and quartz, have been extensively investigated due to their efficient charge trapping mechanisms and well-characterized TL properties, in particular for high-dose radiation sensitivity [1–5]. Several studies of natural and synthetic minerals have been based on the high and very high sensitivity to ionizing radiation, such as aqua marina, tourmaline, LiF, and $CaSiO_3$ [6–10]. Nevertheless, limitations still exist regarding sensitivity, thermal stability, and signal fading, especially in applications involving high radiation doses. As a result, the search for alternative TL materials with improved stability, high-dose linearity, and resistance to environmental degradation remains a key area of research.

Prehnite ($Ca_2Al(AlSi_3O_{10})(OH)_2$) is a naturally occurring calcium-aluminum silicate mineral that has recently gained interest for its defect center studies and potential dosimetric applications [11,12]. Its stable layered structure and resistance to thermal degradation make it a strong candidate for high-dose gamma radiation monitoring. Previous studies have suggested that the presence of transition metal ions, such as Fe^{3+} and Mn^{2+}, can significantly influence TL sensitivity by acting as

* Corresponding authors.
** Corresponding authors. Universidad Nacional de San Agustín de Arequipa, Av. Independencia S/N, Arequipa, Peru.
*** Corresponding authors.
**** Corresponding author. Universidad Nacional de Piura UNP, Miraflores S/N, Piura, Peru.
***** Corresponding author. Instituto de Pesquisas Energéticas e Nucleares, IPEN-CNEN/SP, São Paulo, SP, Brazil.
E-mail addresses: monisebrito@usp.br (M.B. Gomes), cgonzaleslo@unsa.edu.pe (C.D. Gonzales-Lorenzo).

https://doi.org/10.1016/j.jpcs.2026.113519
Received 4 November 2025; Received in revised form 21 December 2025; Accepted 5 January 2026
Available online 6 January 2026
0022-3697/© 2026 Elsevier Ltd. All rights are reserved, including those for text and data mining, AI training, and similar technologies.

charge trapping and recombination centers [13,14]. Additionally, the ability of the prehnite sample to maintain its crystalline integrity after exposure to high temperatures suggests that it could be a suitable material for dosimetry in extreme conditions, where traditional dosimeters may lose effectiveness.

One of the critical factors in evaluating a material for radiation dosimetry is its TL response, which is governed by charge trapping mechanisms, recombination efficiency, and fading characteristics. Studies on silicate minerals have demonstrated that controlled annealing processes can optimize TL sensitivity by modifying defect centers, enhancing charge carrier trapping, and reducing unwanted recombination centers [15,16]. Moreover, previous research on feldspar, quartz, and other silicates has displayed that deep trap levels contribute to long-term signal stability, which is crucial for retrospective dosimetry and prolonged exposure monitoring [3,9,17,18]. Another essential aspect of TL material is its ability to maintain a measurable and reproducible response over time. Fading, or the loss of stored charge over time, is a well-known challenge in radiation dosimetry, particularly for materials with shallow trap levels [2,19,20]. Electron paramagnetic resonance (EPR) spectroscopy has been widely used to study the stability of radiation-induced defect centers, providing complementary insights into charge carrier dynamics that affect TL response [21]. Furthermore, a correlation of TL and EPR data enables a more precise characterization of the defect structure and charge-trapping mechanisms. In aluminosilicate thermoluminescent phosphors, the trapping and subsequent release of radiation-induced charge carriers are controlled by intrinsic and extrinsic point defects within the framework lattice. Under ionizing radiation, electrons and holes are generated and subsequently captured by anion and cation vacancies, interstitials, and substitutional impurity sites, giving rise to classical Frenkel- and Schottky-type defect pairs that function as charge traps and recombination centers [22,23].

Despite the growing interest in alternative dosimetric materials, there remains a significant gap in the systematic study of TL behavior in prehnite samples under controlled thermal treatments and high radiation doses. Most previous research on natural silicates has focused on feldspar and quartz, leaving prehnite relatively unexplored in this context. In TL analysis, kinetic parameters are commonly extracted using classical single-curve procedures such as the initial-rise (IR) method, which exploits the low-temperature exponential part of the glow peak and is largely insensitive to the kinetic order, and peak-shape (PS) techniques based on Chen-type relations between peak geometry and trap depth/order [2,24,25]. Multi-curve strategies, including various-heating-rate (VHR) protocols and computerized glow-curve deconvolution (CGCD), improve the internal consistency of the retrieved parameters and are particularly suitable for complex, multi-peak systems [26,27]. More recently, alternative modelling frameworks have been proposed in which the full TL rate-equation system is solved assuming a sigmoid-type evolution of trapping and recombination centers during irradiation, providing a physically motivated approach for the analysis of experimental TL glow curves of the kind considered here [28–30].

Thus, this study aims to provide a comprehensive structural and luminescent analysis of prehnite using XRF, XRD, EPR, and TL spectroscopy. By investigating the effects of thermal treatment and gamma irradiation on TL response, charge trapping mechanisms, and kinetic parameters, we seek to establish prehnite as a viable dosimetric material for high-radiation environments, contributing to the advancement of alternative silicate-based dosimeters.

2. Experimental details

The prehnite sample investigated in this work was purchased from the LEGEP stone store in São Paulo, Brazil. A large fragment, approximately 5 cm in diameter, was crushed and sieved to obtain grains between 80 and 180 μm for thermoluminescence (TL) and electron paramagnetic resonance (EPR) analyses. In contrast, finer particles (<80 μm) were reserved for XRD.

A commercial X-ray diffractometer (Rigaku Miniflex 600) equipped with CuKα radiation was used to assess the crystal structure. XRD data in the range of $20^\circ \leq 2\theta \leq 80^\circ$, with steps of 0.02°, were recorded. The XRD patterns of all samples were analyzed by the Rietveld method using the GSAS software program. During the process of refinement, all the parameters, such as lattice parameters, peak profile parameters (shft, Lx, GU, GV, GW, S/L, etc.), atomic coordinates (x, y, z, U, and occupancy), were varied.

Before irradiation, all samples underwent annealing at 200, 400, 600, and 800 °C for 60 min in an ambient atmosphere to eliminate residual TL signals and stabilize charge trapping states. XRD was employed to analyze the crystalline structure of prehnite before and after thermal treatments, assessing its structural integrity and any phase transitions induced by heating. Gamma irradiations were conducted at the Radiation Technology Center (CTR) at the Institute for Energy and Nuclear Research (IPEN) using a Co-60 source. The dose rates applied were 2.04 kGy/h for low-dose exposures and 0.47 kGy/h for high-dose exposures. All irradiations were performed at room temperature under conditions of electronic equilibrium.

The TL measurements were performed in a nitrogen atmosphere using a Harshaw model 4500. Luminescence was detected by a Hamamatsu R647 photomultiplier tube through a Schott KG1 filter (transmission band 330–690 nm). The heating rate was set to 4 °C/s, and background subtraction was applied for each measurement. Each glow curve data point represents the average of five readings using a mass of about 1.8 mg of grain (80–180 μm). To ensure peak stability, most TL readings were conducted more than 24 h post-irradiation, except in fading studies, where periodic measurements were performed to assess signal decay over time.

EPR measurements were conducted at room temperature using a Bruker EMX spectrometer with a rectangular cavity (ST-ER4102), operating at 9.75 GHz (X-band) with a microwave power of 20 mW and a modulation field of 100 kHz.

Chemical analysis of the prehnite sample was performed at the Laboratory of Technological Characterization (LCT), Polytechnic School, University of São Paulo, using a PANalytical Zetium X-ray fluorescence (XRF) spectrometer. The sample was analyzed as an anhydrous lithium tetraborate–fused bead using the ROC-1 (rocks) calibration. Loss on ignition (LOI) was determined at 1020 °C for 2 h. Major oxides are reported in wt.% with an estimated uncertainty below 5 %.

Electron paramagnetic resonance (EPR) spectroscopy was applied to investigate paramagnetic centers associated with structural defects. These measurements were performed to identify and characterize charge trapping mechanisms relevant to the thermoluminescent response.

Thermoluminescence (TL) analyses were conducted to study the dosimetric properties of prehnite. The TL response was examined as a function of radiation dose and storage time. Kinetic parameters of TL peaks were determined using the TM-Tstop method to estimate trap activation energies, while glow-curve deconvolution techniques were employed to resolve individual TL components. First- and second-order kinetic models were used to describe charge recombination mechanisms. Fading studies were carried out to assess the temporal stability of TL peaks, with samples stored under controlled conditions and measured at specific time intervals. Additional experiments with varying heating rates were conducted to examine the influence of thermal treatments on the luminescent response.

3. Results and discussion

3.1. X-rays fluorescence

The prehnite sample investigated in this work shows a greenish

coloration, with a variable hue depending on the presence of impurities. This sample presents a light green color, as shown in Fig. 1. XRF analysis of the prehnite sample revealed that the dominant components are SiO_2 (43.0 %), Al_2O_3 (22.3 %), and CaO (27.6 %), which collectively form a robust matrix supporting high thermal stability and effective charge trapping as displayed in Table 1. The presence of Fe_2O_3 (1.82 %) is particularly significant, with a low concentration of MnO (<0.10 %). Similar results have been found by Cairncross et al. (2000) [31]. These authors have shown that microprobe and XRF analyses of prehnite mineral from South Africa reveal typical chemical compositions such as SiO_2, Al_2O_3, and CaO with very low FeO and Na_2O contents, and MnO (±0.4 wt%).

In this work, the main presence of SiO_2, Al_2O_3, and CaO in the prehnite mineral makes its study and subsequent use as a radiation dosimeter of great interest to the scientific community. This is because various studies on materials such as Al_2O_3 and $CaSiO_3$ have demonstrated their potential and continued use as radiation detectors using techniques such as TL and OSL [5,18,19,32–35].

3.2. X-ray diffraction studies

Thermal treatments were carried out on the prehnite samples, which were in powder form, at 400 °C, 600 °C, and 800 °C for 1 h. Fig. 2(a)–(d) shows the X-ray diffraction pattern along with Rietveld refinement obtained for all samples. This analysis reveals the presence of Prehnite compound ($Ca_2Al_2Si_3O_{10}(OH)_2$) as the majority phase with an orthorhombic structure and P2cm space group. Spurious reflections belonging to calcium carbonate compounds ($CaCO_3$) were also observed. Calcite and Vaterite phases were identified; the latter was observed only for samples treated at temperatures of 200 °C and 600 °C. Both phases belong to the rhombohedral space group *R3c*, but with very different lattice parameters.

From Rietveld refinement, the background for the natural sample is more pronounced when compared with the other samples. Indeed, the XRD pattern background for this sample was described in terms of a sixteenth-order polynomial, whereas for the other samples we have used a twelfth-order polynomial. Amorphous crystals appear as a background on the diffraction pattern. We believe that amorphous calcium carbonate compounds are present in the natural sample. The crystallization of the calcite and vaterite phases is achieved by heat treatments. Fig. 2(c) shows the Bragg peaks positions for the three observed phases. The (111) reflection corresponds to the most intense peak of the Vaterite phase. This reflection disappears for samples with T = 200 °C and 600 °C. The (104) reflection localized at 29.4° (2θ) corresponds to the most intense peak of the Calcite phase, whereas the other reflections belong to the Prehnite phase. Furthermore, it is observed that Bragg reflections are very narrow, revealing the bulk size of the grains. From Fig. 2(d), we can see that the unit cell volume decreases with the heat treatment temperature for both Prehnite and Calcite phases.

Fig. 1. Natural prehnite, with a characteristic light green colorused, used in this study. (For interpretation of the references to color in this figure legend, the reader is referred to the Web version of this article.)

Table 1
Main oxide compounds of the prehnite sample.

Components	P1
SiO_2 (%)	43
Al_2O_3 (%)	22.3
Fe_2O_3 (%)	1.82
MnO (%)	<0.10
MgO (%)	0.1
CaO (%)	27.6
Na_2O (%)	0.1
K_2O (%)	<0.10
TiO_2 (%)	<0.10
P_2O_5 (%)	<0.10
LOI (%)	5.29

Values of lattice parameters, composition, and quality factors from refinement are given in Table 2. The values of lattice parameters for both Prehnite and Calcite phases decrease due to the heat treatment. This result is in agreement with the behavior observed for the unit cell volume. The goodness of refinement is judged from S = Rwp/Re and X2 parameters, which indicate that the obtained parameters are accurate.

The reduction of the crystal cell volume suggests that the distances between atoms tend to decrease after heat treatments. This can change the local environment of defect centers, altering their energy gap. On the other hand, it is well known in the literature that calcium carbonate compounds display robust luminescent properties [36–38]. We believe that both the reduction in the unit cell volume and the presence of $CaCO_3$ compounds improve the luminescence properties in our prehnite samples.

3.3. EPR measurements

The EPR spectrum of natural prehnite, shown in Fig. 3, provides insight into the paramagnetic species present in the crystal structure. The spectrum reveals distinct features that indicate the contributions of both Fe^{3+} and Mn^{2+} ions. A distinctive line at $g = 4.0$ is associated with Fe^{3+} in distorted octahedral coordination. This pattern reflects the influence of crystal distortion on the chemical environment of iron, as described by Zandona et al. [39].

Additionally, multiple peaks in the region around $g = 2.0$ are attributed to Mn^{2+}, which presents a hyperfine interaction with I = 5/2, resulting in six regularly spaced lines. These signals reinforce the mixed contribution of manganese and iron ions to the EPR spectrum of prehnite, as suggested by previous studies. Besides, an examination of the EPR spectrum in the $g = 2.0$ region reveals that a low-intensity, broad line overlaps the six-line EPR spectrum. The line width of the broad line is about 470 Gauss, and the *g*-value is estimated to be 1.990. The wide line may be attributed to the presence of Fe^{3+} ions at locations of relatively high symmetry. A simulated spectrum with contributions from Mn^{2+} and Fe^{3+} ions is shown in Fig. 4. The studies mentioned indicate that factors such as the presence of weakly bound water, heating, and irradiation processes can influence the intensity and width of the lines associated with Fe^{3+}. These spectral variations, observed in natural minerals, were also identified in the current analysis, showing similarities with previously studied samples.

Irradiation of prehnite samples with varying doses of gamma radiation did not yield a significant increase in the EPR signal for Fe^{3+} and Mn^{2+} ions. This can be explained by the stability of the electronic states of these ions in specific crystallographic environments, limiting the creation of new paramagnetic centers even with increasing radiation doses. Furthermore, the saturation of defect centers and the possible recombination or relaxation of these defects contribute to the lack of growth in the EPR signal [21]. Thus, the observed EPR spectra are

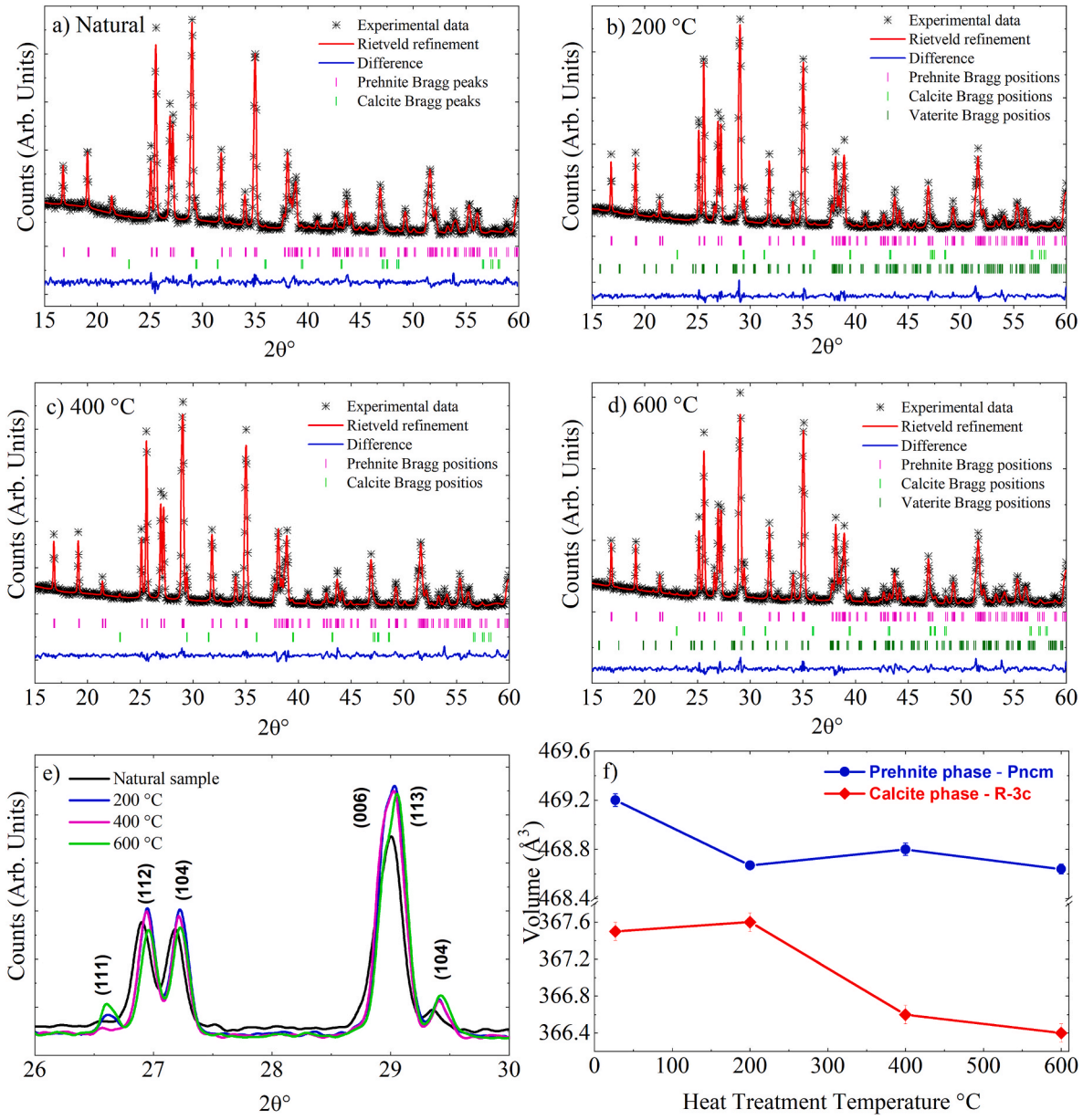

Fig. 2. X-ray powder diffraction along with Rietveld refinement for (a) natural sample, and heat-treated samples with (b) T = 200 °C, (c) 400 °C, and (d) 600 °C. (e) Bragg peaks positions for Prehnite, Calcite, and Vaterite compounds. (f) The unit cell volume as a function of heat treatment temperature for Prehnite and Calcite phases.

consistent with the presence of Fe^{3+} and Mn^{2+} ions in different crystallographic environments in prehnite.

In this section, it is essential to note that in the natural prehnite, $Ca_2Al(AlSi_3O_{10})(OH)_2$, the structural OH groups give rise to intrinsic metal–hydroxyl (M–OH) complexes that can be actively involved in luminescence processes under high-dose irradiation.

García-Guinea et al. proposed that, in insulating materials with metal–hydroxyl surface terminations, the oxygen species responsible for the UV–green cathodoluminescence bands most likely originate from a nonspecific radiolytic process described by the reaction: electron beam + 2(Metal–OH) → H_2O + O + photons [40]. In other hand, calcium in crystalline systems such as calcite ($CaCO_3$) and pseudowollastonite ($CaSiO_3$) forms materials that exhibit high sensitivity to gamma and X-ray irradiation. These crystalline structures contain defect centers such as O^-, F^+, and Ti^{3+} centers. Within the framework of the present TL–EPR investigation, it is therefore reasonable to assume that OH-related centers and other defect centers related to the presence of calcite in prehnite form part of the trapping/recombination network. These distributions may contribute to the broad TL band observed around 550 and 530 nm, together with other intrinsic lattice and impurity-related defects [5,9,18,35–37,41].

3.4. Thermoluminescence results

The thermal treatment procedure on the prehnite samples was performed to optimize their TL response. Fig. 5 presents the TL glow curves of the prehnite sample irradiated with 1 kGy of gamma dose, both naturally and after thermal treatments carried out at 400 °C, 600 °C, and 800 °C. TL glow curves for all samples, except the sample with previous thermal treatment of 800 °C, display three main peaks at 145 °C, a prominent peak at 250 °C, and a high-temperature peak at 362 °C. Among these, the peak located at approximately 250 °C stands out, as it shows the highest TL emission intensity at all different temperatures. This peak is considered thermally stable, as it is associated with deep

Table 2
Lattice parameters, composition and quality factors obtained from Rietveld refinement.

Phase Symmetry	Prehnite *P2cm*	Calcite *R3c*	Vaterite *R3c*
NATURAL			
a (Å)	4.627(1)	4.988(3)	Not observed
b (Å)	5.484(1)	4.988(3)	Not observed
c (Å)	18.490(2)	17.06(2)	Not observed
Composition (fract. %)	98.87(1)	1.13(1)	Not observed
R_p (%)	5.68	5.68	Not observed
R_{wp} (%)	7.51	7.51	Not observed
$S = R_{wp}/R_p$	1.32	1.32	Not observed
X^2	1.59	1.59	Not observed
T = 200 °C			
a (Å)	4.6275(1)	4.979(2)	7.235(1)
b (Å)	5.4815(3)	4.979(2)	7.235(1)
c (Å)	18.477(1)	17.13 (1)	25.26(1)
Composition (fract. %)	86.5(1)	2.5(2)	11.0(2)
R_p (%)	6.26	6.26	6.26
R_{wp} (%)	8.27	8.27	8.27
$S = R_{wp}/R_p$	1.32	1.32	1.32
X^2	1.98	1.98	1.98
T = 400 °C			
a (Å)	4.6261(3)	4.983(2)	Not observed
b (Å)	5.4826(3)	4.983(2)	Not observed
c (Å)	18.481(1)	17.05(1)	Not observed
Composition (fract. %)	97.01(2)	2.99(2)	Not observed
R_p (%)	6.35	6.35	Not observed
R_{wp} (%)	8.69	8.69	Not observed
$S = R_{wp}/R_p$	1.37	1.37	Not observed
X^2	1.98	1.98	Not observed
T = 600 °C			
a (Å)	4.6268(3)	4.982(1)	7.244(2)
b (Å)	5.4809(3)	4.982(1)	7.244(2)
c (Å)	18.481(1)	17.043(3)	25.29(3)
Composition (fract. %)	91.3 (1|)	2.1(1)	6.6(3)
R_p (%)	6.45	6.45	6.45
R_{wp} (%)	8.47	8.47	8.47
$S = R_{wp}/R_p$	1.31	1.31	1.31
X^2	1.97	1.97	1.97

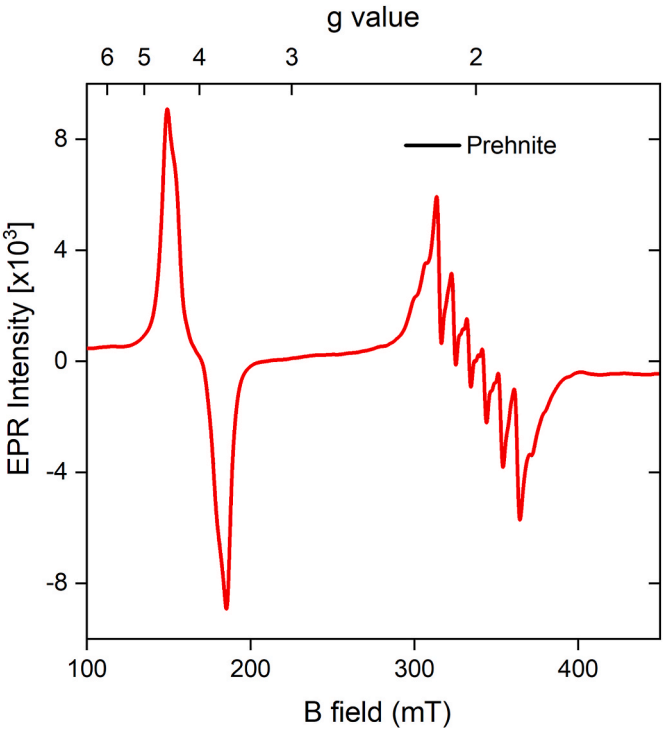

Fig. 3. EPR spectrum of natural prehnite showing contributions from Fe^{3+} and Mn^{2+} ions, with distinctive lines at about g = 4.0 and g = 2.00, respectively.

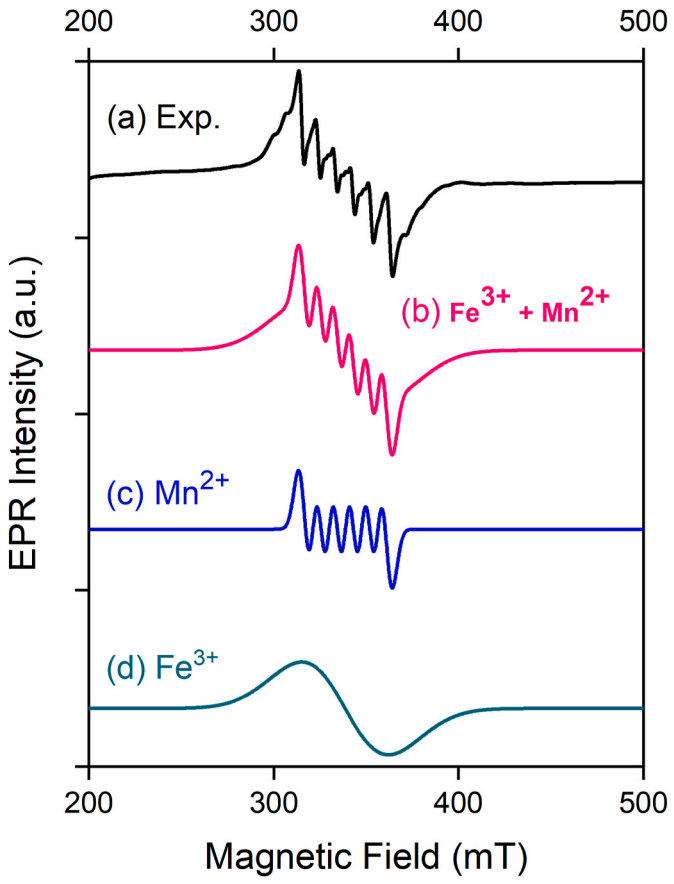

Fig. 4. (a) Room temperature EPR spectrum observed from the prehnite sample. (b) Simulated spectrum with contributions from Mn^{2+} and Fe^{3+} ions, (c) simulated spectrum only from Mn^{2+} ion, and (d) simulated spectrum from Fe^{3+} ion.

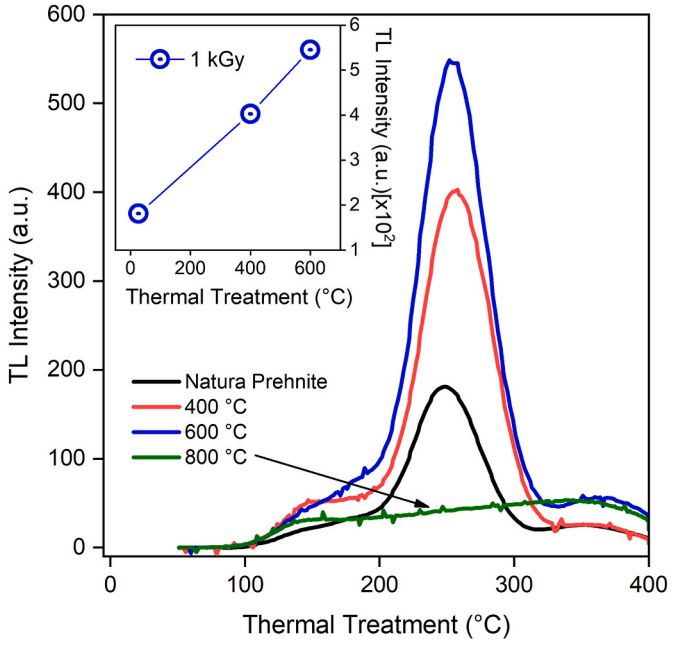

Fig. 5. TL glow curves of natural prehnite and those thermally treated at 400, 600, and 800 °C, irradiated with a 1 kG dose of gamma radiation.

traps capable of retaining charges for prolonged periods before their

thermal release. On the other hand, the peaks located below 200 °C are classified as unstable, since they correspond to shallow traps that are susceptible to the spontaneous release of electrons even at room temperature, which compromises the retention of dosimetric information [2].

As can be seen in Fig. 5, the response of the sample with a thermal treatment of 400 °C already promotes a slight increase in TL intensity compared to that of natural prehnite, indicating partial activation of trapping centers in the material. However, the treatment at 600 °C stands out for generating the most intense response, with a well-defined peak around 250 °C. This thermal condition appears to favor the organization of the crystalline structure, creating or stabilizing electronic traps that result in greater efficiency in TL emission. On the other hand, thermal treatments at 800 °C result in a significant decrease in TL intensity. Complementary XRD analyses have indicated that thermal treatment starting at 800 °C compromises the structural integrity of the prehnite, which no longer exhibits its typical crystallographic characteristics. Therefore, this temperature is excessive and promotes irreversible changes that negatively impact the ability to store and release energy through the thermoluminescent process. In the inset of Fig. 5, it can be seen that at temperatures of 400 °C and 600 °C, there is an increase in the intensity of TL with respect to the natural sample of approximately 55 % and 67 %, respectively. Consequently, the sample heat-treated at 600 °C for 1 h was selected for subsequent analyses, since it showed the highest thermoluminescent response, indicating greater sensitivity to gamma radiation. Hereafter, the natural prehnite sample heat-treated at 600 °C will be referred to as the sample under study.

To evaluate the dose dependence of TL for the heat-treated prehnite sample, it was irradiated with gamma doses ranging from 100 Gy to 100 kGy. TL glow curves of the sample irradiated with gamma radiation with doses from 100 Gy to 8 kGy are shown in Fig. 6(a), whilst TL glow curves with doses from 9 kGy to 100 kGy are shown in Fig. 6(b). TL glow curves show peaks at approximately 170, 245, and 325 °C, increasing with the irradiation gamma dose.

An important property to consider in TL analysis is fading [2]. Fading analysis of the prehnite sample, after thermal treatment at 600 °C for 1 h, followed by irradiation with a 10 kGy gamma dose, revealed a complex decay behavior of the TL intensity. Experimental TL peaks at 130, 240, and 350 °C are present as shown in the inset of Fig. 7.

The TL intensity at 130 °C shows a rapid decrease, losing approximately 96.83 % of its initial intensity within the first 117 h of storage, as shown in Fig. 7. The 240 and 350 °C TL peaks have shown a more gradual decay, losing around 40 % of their TL intensity after 130 h and stabilizing afterward. These high-temperature (beyond 200 °C) peaks have demonstrated higher stability, retaining a significant portion of their intensity even after prolonged storage times. These results suggest that deeper traps, associated with higher temperature peaks, are more stable and less prone to fading over time.

Fig. 8 (a) presents the variation of TL intensity of prehnite samples as a function of gamma radiation dose (kGy), in a double logarithmic (log-log) scale. The curves correspond to TL peaks observed at 170 °C (black squares), 245 °C (red circles), and 325 °C (blue triangles). Dashed lines with a 45° slope were included as references for ideal linear behavior between TL intensity and dose. The comparison between experimental curves and these reference lines allows identification of linear, supralinear, sublinear, and saturation regimes, as described by McKeever [2]. The 170 °C TL peak shows unstable behavior with a possibly sublinear trend at lower doses (<2 kGy), followed by an approximately linear region between 4 and 10 kGy, where the curve remains close to the 45° slope. For doses above 10 kGy, a reduction in the slope is observed, indicating a transition to a sublinear regime that culminates in saturation at about 30 kGy. After that, the TL response displays decreasing behavior in the value (curve) up to 100 kGy, as shown in Fig. 8 (a). On the other hand, the 245 °C TL peak exhibits linear behavior between 0.1 and 2 kGy, as evidenced by good agreement with the unit slope line. Beyond this point, a pronounced sublinearity is observed, with TL

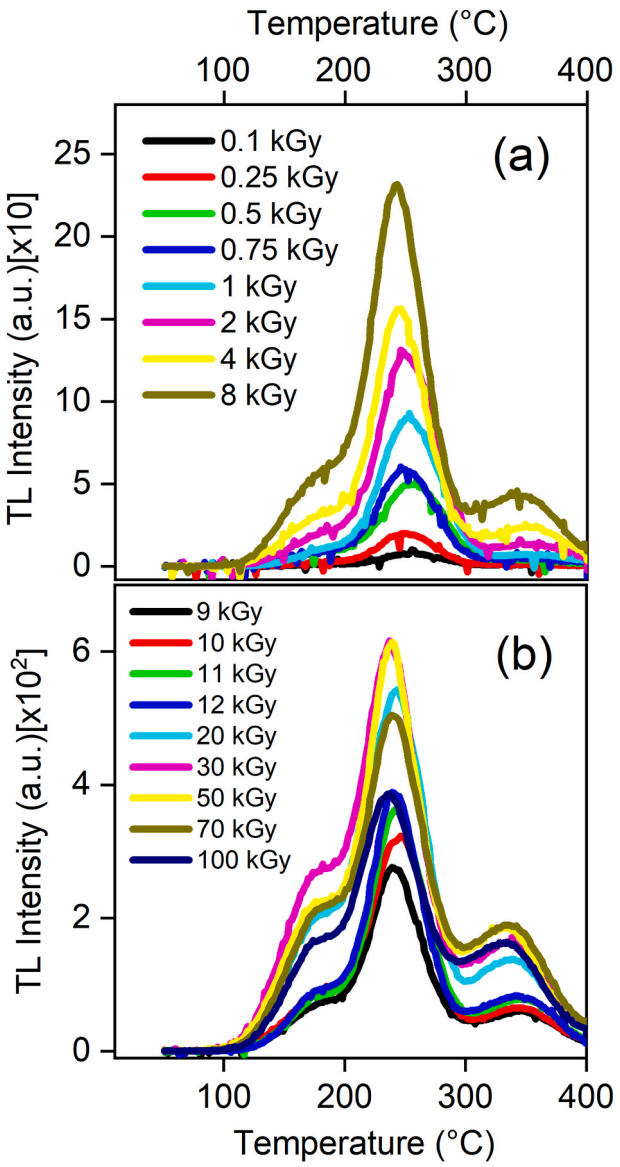

Fig. 6. TL curves of natural prehnite treated at 600 °C and irradiated with doses from 0.1 to 100 kGy. An increase in emission is observed up to 30 kGy, followed by a gradual decrease from 50 kGy onwards. The main peak remains at approximately 245 °C.

intensity decreasing more than proportionally with dose. This effect may be due to the decrease in available traps within the material, which can no longer retain the absorbed radiation energy. The sublinearity behavior extends up to around 30 kGy, where saturation is achieved. After that, a decreasing response with the dose is observed up to 100 kGy, similarly to the 170 °C TL peak. Finally, the 325 °C TL peak exhibits moderate TL response, with a linear behavior from 0.5 to 20 kGy. After that, a saturation process is observed between 30 and 100 kGy. This behavior suggests that the trapping centers activated in this thermal region are more thermally stable but less efficient or less abundant. The comparative analysis of these TL peaks, based on the 45° reference line, indicates that the 245 °C and 325 °C TL displays sensitivity, linearity, and a wide dynamic response range in the radiation dose. These results reveal the potential use of the prehnite sample as a dosimeter for intermediate-high radiation doses.

For the TM-Tstop method, TL readings for the prehnite sample irradiated with 10 kGy were performed, following for each measurement the sequence of thermal treatment and subsequent TL reading. The

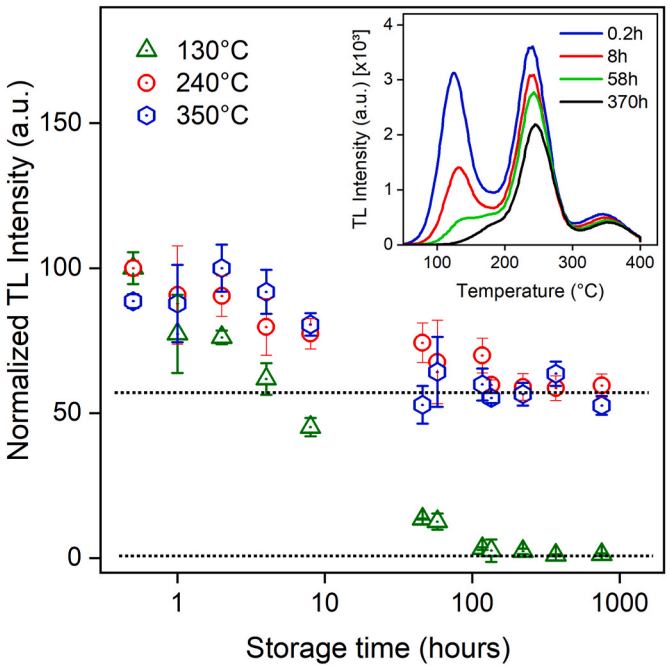

Fig. 7. Fading behavior of the prehnite sample under storage conditions.

thermal treatment was applied incrementally, in 5 °C steps, starting at 55 °C and continuing up to 335 °C. The initial part of the TL glow curve can be described by exponential behavior as exp(-E/kT), but considering points on the curve below 15 % of the maximum TL intensity [42]. This method is called the initial rise method. The obtained values ranged from 1.07 to 1.55 eV, corresponding to the different stabilization regions of the TL peaks, as can be seen in Fig. 9. These results demonstrate that the traps in the material require different amounts of energy to release the trapped electrons, which is manifested in the multiplicity of the observed TL peaks.

The experimental TL glow curve was analyzed by glow-curve deconvolution using a dedicated software package that separates the measured signal into a set of individual glow peaks. In this work, we employed the open-source CGCD (Computed Glow Curve Deconvolution) implementation GCD Analyzer, which uses TL peak expressions based on improved rational approximations [43]. Kinetic parameters were obtained by fitting a composite model consisting of five components, guided by the prior T_M–T_{stop} and E–T_{stop} analyses. Components 1, 4, and 5 were described with a second-order kinetics (SOK) formalism assuming a discrete set of trapping centers, whereas components 2 and 3 were modeled using a continuous trap distribution under first-order kinetics (FOK), consistent with the T_M–T_{stop} results. The deconvolution yielded five TL components, with TL peaks at approximately 167, 247.4, 265, 293, and 346 °C, with activation energies of 1.07, 1.22, 1.32, 1.49, and 1.55 eV, respectively.

Beyond well-defined discrete traps, a wide range of aluminosilicates, particularly feldspars and aluminosilicate glasses, display TL/OSL signals better described by a near-continuous distribution of trap depths (or thermal stabilities) than by a few isolated levels [44]. This behavior is typically attributed to structural and compositional disorder, which gives rise to localized/band-tail states within aluminosilicate frameworks. Consequently, when TL peaks are broad and shift with preheating, it is physically justified to include continuous trap distribution (CTD) terms, either alone or together with discrete components, within CGCD-based glow-curve deconvolution [45,46]. FOM of 2.60 % was obtained from the fitting, indicating good agreement between the experimental data and the applied theoretical model.

To perform a more robust and comprehensive dose–response analysis, we evaluate the dose dependence of the TL intensity associated

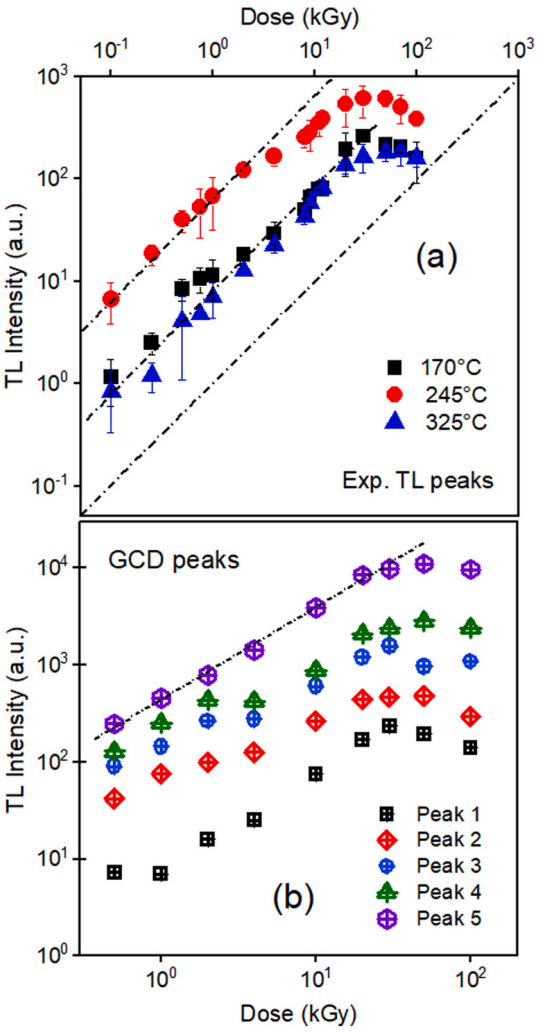

Fig. 8. (a) TL intensity behavior of the 170, 245, and 325 °C peaks as a function of gamma radiation doses; dashed lines indicate linearity. (b) Dose–response curves of the TL peaks obtained from glow-curve deconvolution (0.5–100 kGy).

with each of the five deconvoluted TL peaks, as shown in Fig. 8(b). For each investigated dose, the corresponding TL glow curve was deconvoluted (GCD) for irradiation doses of 0.5, 1, 2, 4, 10, 20, 30, 50, and 100 kGy. To display the dose dependence of each DGC component separately, the individual dose-response curves were vertically shifted. Therefore, the plotted intensities are intended for comparative visualization only, as can be seen in Fig. 8(b). By analyzing the dose dependence of each trap, Peak 1 exhibits an approximately linear response from 4 to 10 kGy, followed by a decrease in TL intensity with increasing dose, closely resembling the behavior observed for the experimental TL peak at 170 °C. In contrast, Peaks 2, 3, and 4 show trends similar to the experimental TL peak near 245 °C, which is approximately linear up to 2 kGy and then becomes sublinear up to 30 kGy, followed by a decay at higher doses. Notably, the prominent experimental TL peak around 245 °C is mainly composed of the individual components Peaks 2, 3, and 4. Finally, Peak 5 displays a linear response from 0.5 to 20 kGy, after which the TL signal reaches saturation, exhibiting a trend consistent with the experimental TL feature centered at about 325 °C. These results provide a more detailed characterization of the dose–response behavior of each GCD TL peak and highlight the promising dosimetric features of the high-temperature peak near 325 °C for high-dose dosimetry applications.

The method of various heating rates (VHR) was also applied to estimate the activation energy (Ea) and frequency factor (s) of the TL

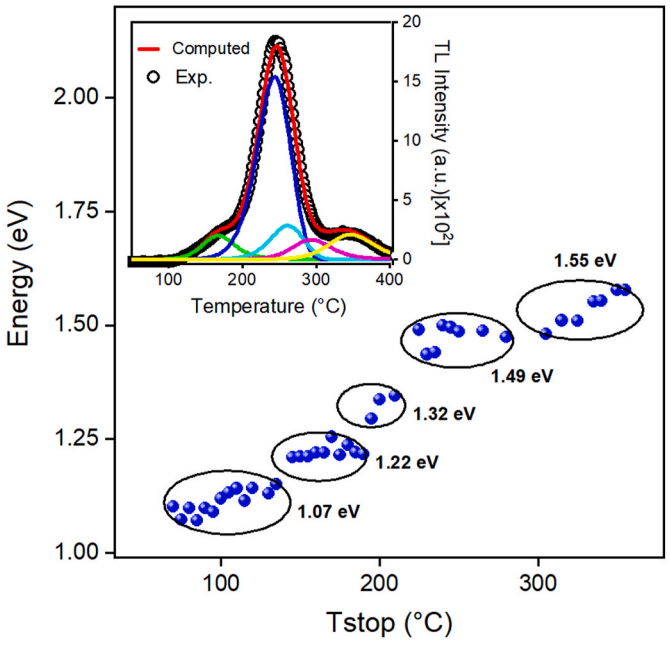

Fig. 9. Activation energies vs. Tstop. The activation energy values range from 1.07 eV to 1.55 eV, corresponding to different temperature ranges. In the inset, the deconvolution of the TL glow curve shows the individual contributions of overlapping peaks.

traps. As shown in Fig. 10, the TL glow curves present systematic shifts in peak temperatures with increasing heating rates β, indicating well-defined trapping mechanisms. The results obtained from the multiple heating rate method indicate that the second experimental TL peak is associated with a thermal activation process involving deep energy traps, which can be evidenced by the continuous increase of Tm with the increment of β. A Ln(Tm/β) versus 1/T (K^{-1}) plot to determine the activation energy of the TL peak was used, as can be seen in the inset in Fig. 10. The linearity observed in this plot confirms that the process

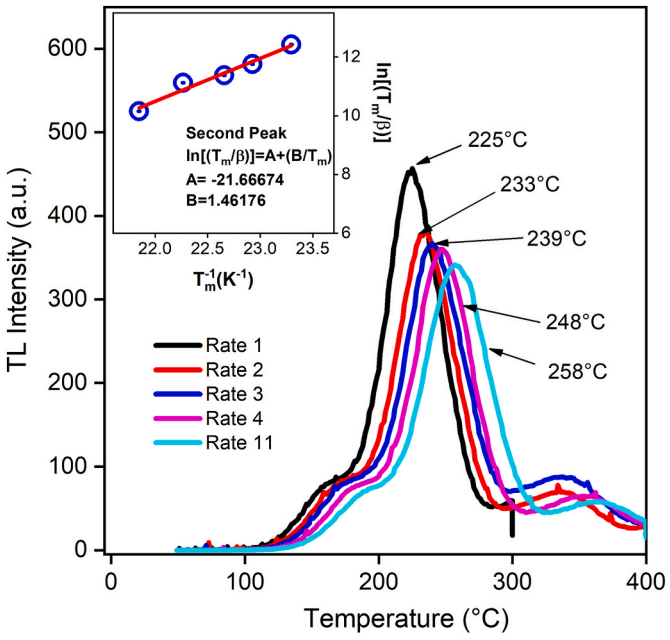

Fig. 10. TL curves of prehnite at different heating rates, showing the shift of glow peaks with increasing temperature. In the inset, a plot of ln(Tm/β) as a function of the inverse temperature (1/T, in K^{-1}) was constructed for the second TL glow peak.

follows first-order kinetics. The activation energy of the second experimental TL glow peak was calculated as 1.46 eV, corroborating the results obtained from the TM-Tstop method. This agreement between complementary methods highlights the reliability of the kinetic parameters and emphasizes the stability of deep traps in prehnite, particularly for dosimetric applications. The positions, activation energies (E), and frequency factors (s) of the TL peaks, obtained by the GCD **and VHR** methods, are summarized in Table 3. It can be observed that the *s* and tau values are close and of the same order of magnitude for both methods used.

The emission peaks were located around 167, 247.4, 265, 293, and 346 °C. The high activation energy associated with the 346 °C peak (1.55 eV) suggests a deeper trapping, providing increased resistance to thermal fading. The dose–response of the deconvoluted TL Peak 5 exhibits behavior similar to that of the experimental peak around 325 °C, demonstrating suitable characteristics for its use as a gamma radiation detector, as shown in Fig. 8 (b).

The TL emission spectrum of the prehnite sample, after gamma irradiation with a dose of 16 kGy, presented two main bands, as shown in Fig. 11 (a). One prominent band, centered at 550 nm, and a lower band at about 530 nm, corresponded to temperatures of 260 and 380 °C, respectively. This behavior suggests the activation of two recombination centers associated with the electronic trap structure of the sample. Since the time elapsed between irradiation and the readout measurements was longer than one week, the low-temperature TL peaks, below 200 °C, did not appear due to the fading effect. Thus, the majority of the contribution comes from photons with wavelengths between 480 and 610 nm, which corresponds to the experimental TL peaks at 240 and 350 °C (as shown in Fig. 6 a).

To better resolve the emission centers contributing to the TL spectrum, Fig. 11(b) shows the TL intensity as a function of wavelength recorded at fixed temperatures. The selected temperatures correspond to the experimental glow-curve maxima at T = 200, 260, and 380 °C, i.e., the temperature regions where the TL spectral output is most pronounced. As evidenced in Fig. 11(b), the spectrum is dominated by two prominent emission bands centered at approximately 530 and 570 nm, in agreement with the features previously identified in the TL spectral analysis. Additionally, weaker bands near 490 and 610 nm are discernible, suggesting the presence of two further radiative recombination (emission) centers with comparatively lower TL yield. The overall emission is maximized at T = 260 °C. By comparison, the peak intensities at 200 and 380 °C are on the order of about 20 % of the maximum intensity observed at 260 °C.

4. Conclusion

XRF analysis of natural prehnite ($Ca_2Al_2Si_3O_{10}(OH)_2$) displays main components as SiO_2 (43.0 %), Al_2O_3 (22.3 %), CaO (27.6 %), Fe_2O_3 (1.82 %), with a low concentration of MnO (<0.10 %). Heat-treatment in prehnite samples at 400 °C, 600 °C, and 800 °C was performed for XRD and TL analysis. XRD patterns were analyzed by Rietveld refinement for all samples. This analysis reveals the majority phase to be Prehnite, characterized by an orthorhombic structure and a P2cm space group. Calcite and vaterite phases were detected in heat treatment samples. Both phases crystallize in the rhombohedral space group *R*3*c*, but with distinct lattice parameters. The lattice parameters of both Prehnite and Calcite phases decrease upon heat treatment, which modifies the local environment of defect centers and, consequently, alters their energy gap.

The EPR spectrum of prehnite shows signals from both Fe^{3+} and Mn^{2+} ions. The line at g = 4.0 corresponds to Fe^{3+} in distorted octahedral coordination, while the six-line pattern near g ≈ 2.00 arises from Mn^{2+} (I = 5/2) due to hyperfine splitting. A weak, broad line overlapping this region is attributed to Fe^{3+} ions in sites of higher symmetry.

TL intensity increased by approximately 55 % and 67 % relative to the natural sample for prior thermal treatments at 400 °C and 600 °C (1

Table 3
TL peak position, activation energy (E), frequency factor (s), and tau (τ, yr at 25 °C) of the TL peaks of the prehnite sample calculated by the GCD and VHR methods.

Peak	Order	TL peak (°C)	E (eV) GCD	s (s^{-1}) GCD	τ GCD	s (s^{-1}) VHR	τ VHR
1	2	167	1.07	$4.58x10^{11}$	0.085	$4.35x10^{11}$	0.089
2	1	247.4	1.22	$1.35x10^{11}$	98.12	$1.90x10^{11}$	69.9
3	1	265	1.32	$4.87x10^{11}$	1338	$5.43x10^{11}$	1200
4	2	293	1.49	$3.96x10^{12}$	$1.23x10^{5}$	$7.56x10^{12}$	$0.64x10^{5}$
5	2	346	1.55	$7.77x10^{11}$	$6.48x10^{6}$	$9.55x10^{11}$	$5.27x10^{6}$

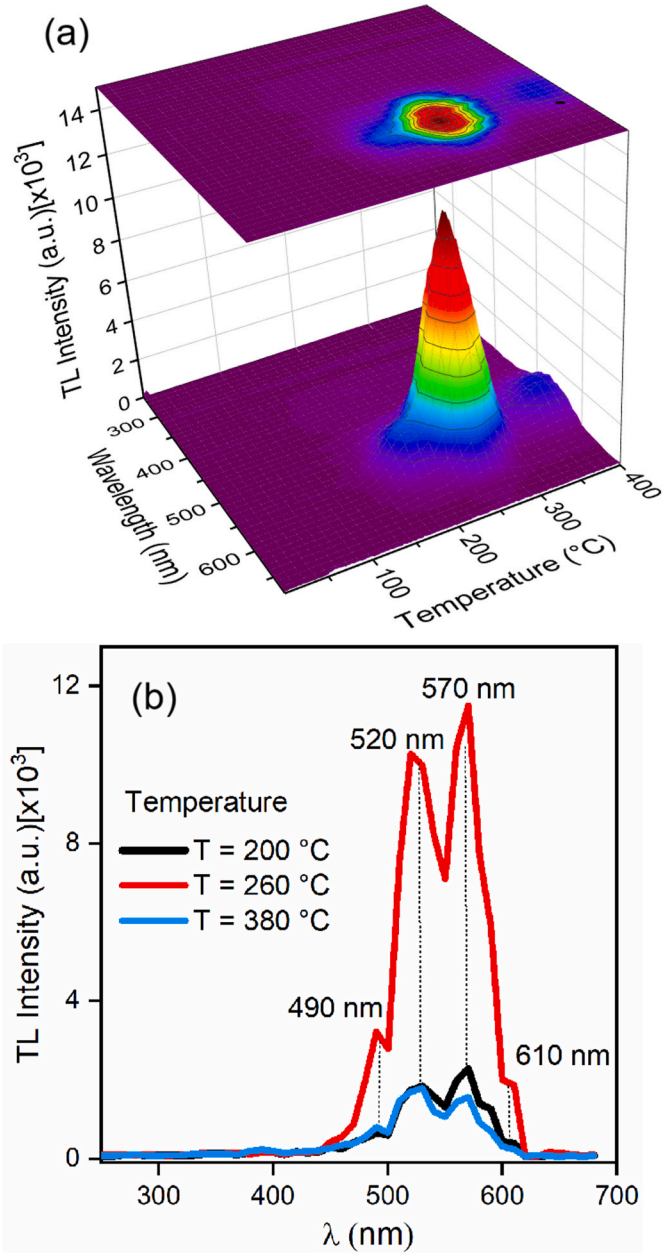

Fig. 11. 3D graph showing the TL intensity of the prehnite sample as a function of temperature and wavelength. The graph displays a very intense 550 nm band and a weak 530 nm band. (b) TL intensity as a function of wavelength measured at the temperature of TL glow-curve maxima (200, 260, and 380 °C).

h), respectively. Consequently, the sample treated at 600 °C was selected for subsequent analyses, as it shows the highest thermoluminescent response. Fading analysis of the prehnite sample irradiation with a 10 kGy gamma dose has displayed a rapid decrease, losing approximately 96.83 % of its initial intensity within the first 117 h of storage, for the TL peak at 130 °C. TL peaks at 240 and 350 °C show a gradual decay, with nearly 40 % of their initial intensity lost after 5.42 days (130 h), after which stabilization was observed. Besides, the prehnite sample was irradiated with gamma doses ranging from 100 Gy to 100 kGy, displaying TL peaks at about 170, 245, and 325 °C. TL response as a function of gamma dose exhibits linear, supralinear, sublinear, and saturation regimes. Mainly, the 245 and 325 °C TL peaks have shown linear behavior for 0.1–2 kGy and 0.5–20 kGy, respectively. Beyond this dose, a sublinear response is observed, extending up to approximately 30 kGy, where saturation occurs. These peaks offer better performance for the intermediate-high radiation gamma dose for dosimetric purposes.

The kinetic parameters of the TL glow peaks were determined using the GCD and VHR methods. GCD has revealed the separation into six main peaks, each associated with a specific recombination process, determined based on the activation energies. Peaks were observed at approximately 167, 247.4, 265, 293, and 346 °C, with the corresponding activation energies of 1.07, 1.22, 1.32, 1.49, and 1.55 eV, respectively. The FOM value calculated from the fitting was 2.60 %, indicating good agreement between the experimental and calculated data.

TL emission spectra of the sample irradiated with 16 kGy gamma-dose revealed a very intense 520 and 570 nm bands and a weak 550 nm band corresponding to 260 and 400 °C TL peaks, respectively. This result suggests the presence of two recombination centers that participate in the TL process. The wavelength-dependent TL response measured at the main glow-curve maxima (200, 260, and 380 °C) is primarily characterized by emission bands near 530 and 570 nm. Additional weaker features are observed around 490 and 610 nm. The highest emission intensity occurs at T = 260 °C.

CRediT authorship contribution statement

Monise B. Gomes: Writing – original draft, Methodology, Investigation. **Carlos D. Gonzales-Lorenzo:** Writing – original draft, Investigation, Data curation. **René R. Rocca:** Data curation, Methodology. **F. N. Ramirez:** Data curation, Conceptualization, Software. **Edy E. Cuevas-Arizaca:** Investigation, Writing – review & editing. **Betzabel N. Silva-Carrera:** Methodology, Data curation. **T.K. Gundu Rao:** Visualization, Investigation, Conceptualization. **Nilo F. Cano:** Writing – review & editing, Visualization. **Jose F.D. Chubaci:** Visualization, Supervision.

Declaration of competing interest

The authors declare that they have no known competing financial interests or personal relationships that could have appeared to influence the work reported in this paper.

Acknowledgment

The authors are very grateful to Ms. E. Somessari and Mr. Aldo Oliviera, Instituto de Pesquisas Energéticas e Nucleares (IPEN/CNEN-SP), for kindly carrying out the irradiation of the samples. To Capes for a fellowship to Monise B. Gomes (Process number 88887.506492/2020-00).

Appendix A. Supplementary data

Supplementary data to this article can be found online at https://doi.org/10.1016/j.jpcs.2026.113519.

Data availability

Data will be made available on request.

References

[1] M.J. Aitken, Thermoluminescence Dating, 1985.
[2] S.W.S. McKeever, Thermoluminescence of Solids, Cambridge University Press, 1985.
[3] K.V.R. Murthy, Thermoluminescence and its applications: a review, Defect Diffusion Forum 347 (2014) 35–73.
[4] R.H. Kars, J. Wallinga, IRSL dating of K-feldspars: modelling natural dose response curves to deal with anomalous fading and trap competition, Radiat. Meas. 44 (2009) 594–599.
[5] C.D. Gonzales-Lorenzo, L.F. Nascimento, S. Kodaira, M.B. Gomes, S. Watanabe, Thermoluminescence studies of polycrystalline CaSiO3 pellets for photons and particle therapy beams, Radiat. Phys. Chem. 177 (2020) 109132.
[6] S. Watanabe, N.F. Cano, L.S. Carmo, R.F. Barbosa, J.F.D. Chubaci, High- and very-high-dose dosimetry using silicate minerals, Radiat. Meas. 72 (2015) 66–69.
[7] B. Obryk, K. Malik, P. Bilski, A. Igielski, J. Dankowski, A. Kurowski, R. Prokopowicz, K.J.R.P.D. Pytel, High-Dose TL Dosimetry of Reactor Neutrons, Radiat. Prot. Dosim. 180 (1–4) (2018) 235–239.
[8] C.D. Gonzales-Lorenzo, S. Watanabe, T.A. Cavalieri, N.F. Cano, T.G. Rao, J. F. Chubaci, L.S. Carmo, C.C.J.R.P. Bueno, Chemistry, Calculated and Experimental Response of Calcium Silicate Polycrystalline to High and very-high Neutron Doses, Radiat. Phys. Chem. 172 (2020) 108820.
[9] C.D. Gonzales-Lorenzo, T.K. Gundu Rao, A.A. Ccollque-Quispe, J. Ayala-Arenas, M. B. Gomes, B.N. Silva-Carrera, R.F. Gennari, V.S. Pachas, F. Monzon-Macedo, H. Loro, J.F.D. Chubaci, N.F. Cano, R.R. Rocca, S. Watanabe, Study of the centers responsible for the TL emission by EPR and PL analysis of Eu-doped CaSiO3 phosphors synthesized by the devitrification method, Mater. Res. Bull. 171 (2024) 112607.
[10] H. Liu, Z. Xiong, Q. Chen, L. Wang, C. Wang, Study on the preservation effect of 60Co-γ ray irradiation on potatoes, Sci. Rep. 14 (2024) 21811.
[11] N. Mironova-Ulmane, V. Skvortsova, A.I. Popov, Optical absorption and luminescence studies of fast neutron-irradiated complex oxides for jewellery applications, Low Temp. Phys. 42 (2016) 584–587.
[12] M. Mao, M.J. Nilges, Y. Pan, Single-crystal EPR and ENDOR study of an Al—O− center in prehnite: implications for aluminum-associated oxyradicals in layer silicates, Eur. J. Mineral 22 (2010) 381–392.
[13] A. Sathyamoorthy, J.M. Luthra, Mechanism of thermoluminescence in magnesium oxide, J. Mater. Sci. 13 (1978) 2637–2644.
[14] M. Abramishvili, Z. Akhvlediani, M. Galustashvili, G. Dekanozishvili, T. Kalabegishvili, V. Kvatchadze, V.J.J.o.M.P. Tavkhelidze, Peculiarities of Radiation Effects in Mgo: Mn 2+ Crystals, J. Mod. Phys. 2 (2011) 2011).
[15] C.D. Gonzales-Lorenzo, D.J. Callo-Escobar, A.A. Ccollque-Quispe, T.K.G. Rao, F.F. H. Aragón, J.C.R. Aquino, D.G. Pacheco-Salazar, H. Loro, J.F. Benavente, J. Mosqueira-Yauri, H.S. Javier-Ccallata, J.S. Ayala-Arenas, N.F. Cano, Effect of annealing temperature on the structural, thermoluminescent, and optical properties of naturally present salt from Lluta region of Peru, Opt. Mater. 126 (2022) 112215.
[16] T. Allard, E. Balan, G. Calas, C. Fourdrin, E. Morichon, S. Sorieul, Radiation-induced defects in clay minerals: a review, Nucl. Instrum. Methods Phys. Res. Sect. B Beam Interact. Mater. Atoms 277 (2012) 112–120.
[17] R.H. Kars, N.R.J. Poolton, M. Jain, C. Ankjærgaard, P. Dorenbos, J. Wallinga, On the trap depth of the IR-sensitive trap in Na- and K-feldspar, Radiat. Meas. 59 (2013) 103–113.
[18] C.D. Gonzales-Lorenzo, T.K.G. Rao, N.F. Cano, B.N. Silva-Carrera, R.R. Rocca, E. E. Cuevas-Arizaca, J.S. Ayala-Arenas, S. Watanabe, Thermoluminescence and defect centers in β-CaSiO3 polycrystal, J. Lumin. 217 (2020) 116783.
[19] V. Kortov, Materials for thermoluminescent dosimetry: current status and future trends, Radiat. Meas. 42 (2007) 576–581.
[20] A.J.J. Bos, High sensitivity thermoluminescence dosimetry, Nucl. Instrum. Methods Phys. Res. Sect. B Beam Interact. Mater. Atoms 184 (2001) 3–28.
[21] M. Ikeya, New Applications of Electron Spin Resonance, 1993.
[22] V. Correcher, Y. Rodriguez-Lazcano, J. Garcia-Guinea, E.J.B.J.o.P. Crespo-Feo, Blue Thermoluminescence Emission of Annealed Lithium Rich Aluminosilicates, Braz. J. Phys 40 (2010) 348–352.
[23] A.A. Finch, H. Friis, M. Maghrabi, Defects in sodalite-group minerals determined from X-ray-induced luminescence, Phys. Chem. Miner. 43 (2016) 481–491.
[24] R. Chen, S.W.S. McKeever, Theory of Thermoluminescence and Related Phenomena, World Scientific, 1997.
[25] G. Kitis, V. Pagonis, Peak shape methods for general order thermoluminescence glow-peaks: a reappraisal, Nucl. Instrum. Methods Phys. Res. Sect. B Beam Interact. Mater. Atoms 262 (2007) 313–322.
[26] R. Chen, J.L. Lawless, V. Pagonis, On the various-heating-rates method for evaluating the activation energies of thermoluminescence peaks, Radiat. Meas. 150 (2022) 106692.
[27] G. Kitis, J.M. Gomez-Ros, J.W.N. Tuyn, Thermoluminescence glow-curve deconvolution functions for first, second and general orders of kinetics, J. Phys. Appl. Phys. 31 (1998) 2636.
[28] J. Benavente, J. Gómez-Ros, A. Romero, Thermoluminescence glow curve deconvolution for discrete and continuous trap distributions, Appl. Radiat. Isot. 153 (2019) 108843.
[29] J.F. Benavente, J.M. Gómez-Ros, V. Correcher, A kinetic model for the thermoluminescent high dose response of LiF:Mg,Cu,P (MCP-N), Appl. Radiat. Isot. 170 (2021) 109634.
[30] M. El-Kinawy, H.F. El-Nashar, N. El-Faramawy, New handling of thermoluminescence glow curve deconvolution expressions for different kinetic orders based on OTOR model, J. Phys. Conf. 1253 (2019) 012012.
[31] B. Cairncross, H. Tsikos, C. Harris, Prehnite from the Kalahari manganese field, South Africa, and its possible implications, S. Afr. J. Geol. 103 (2000) 231–236.
[32] J.C. Mittani, M. Prokić, E.G. Yukihara, Optically stimulated luminescence and thermoluminescence of terbium-activated silicates and aluminates, Radiat. Meas. 43 (2008) 323–326.
[33] A. Pradhan, P.K.D. Sharma, V.K.J.R.P.D. Shirva, Thermoluminescence Response of AL2O3:C to UV and Ionising Radiation, Radiat. Prot. Dosim. 64 (3) (1996) 227–231.
[34] C.D. Gonzales-Lorenzo, D.V. Ananchenko, S.V. Nikiforov, A.N. Kiryakov, A. F. Zatsepin, J.F.D. Chubaci, N.F. Cano, J.S. Ayala-Arenas, S. Watanabe, Effect of 130 keV pulsed electron irradiation on the efficiency of radiative transitions in Eu-doped glass-ceramics CaSiO3, Opt. Mater. 119 (2021) 111304.
[35] C.D. Gonzales-Lorenzo, S. Watanabe, N.F. Cano, J.S. Ayala-Arenas, C.C. Bueno, Synthetic polycrystals of CaSiO3 un-doped and Cd, B, Dy, Eu-doped for gamma and neutron detection, J. Lumin. 201 (2018) 5–10.
[36] E. Isik, D. Toktamis, M.B. Er, M. Hatib, Classification of thermoluminescence features of CaCO3 with long short-term memory model, Luminescence 36 (2021) 1684–1689.
[37] J.M. Kalita, M.L. Chithambo, Thermoluminescence and infrared light stimulated luminescence of limestone (CaCO3) and its dosimetric features, Appl. Radiat. Isot. 154 (2019) 108888.
[38] W.E. Graves, H.H. Roberts, Thermoluminescence spectral shifts of some naturally occurring calcium carbonates, Chem. Geol. 9 (1972) 249–256.
[39] A. Zandonà, V. Castaing, A.I. Shames, G. Helsch, J. Deubener, A.I. Becerro, M. Allix, A. Goldstein, Oxidation and coordination states assumed by transition metal dopants in an invert ultrabasic silicate glass, J. Non-Cryst. Solids 603 (2023) 122094.
[40] J. Garcia-Guinea, F. Garrido, P. Lopez-Arce, V. Correcher, J. de la Figuera, Spectral green cathodoluminescence emission from surfaces of insulators with metal-hydroxyl bonds, J. Lumin. 190 (2017) 128–135.
[41] Y.A. Abdel-Razek, Thermoluminescence dosimetry using natural calcite, J. Taibah Univ. Sci. 10 (2016) 286–295.
[42] P. Kivits, H.J.L. Hagebeuk, Evaluation of the model for thermally stimulated luminescence and conductivity; reliability of trap depth determinations, J. Lumin. 15 (1977) 1–27.
[43] M. Wazir-ud-Din, S. ur-Rehman, M.M. Mahmood, K. Ahmad, S. Hayat, M. T. Siddique, M.B. Kakakhel, S.M. Mirza, Computerized glow curve deconvolution (CGCD): a comparison using asymptotic vs rational approximation in thermoluminescence kinetic models, Appl. Radiat. Isot. 179 (2022) 110014.
[44] J. Gomez-Ros, V. Correcher, J. Garcia-Guinea, A.J.R.p.d. Delgado, Evolution of the Trapped Charge Distribution due to Trap Emptying Processes in a Natural Aluminosilicate, Radiat. Prot. Dosim. 119 (1–4) (2006) 93–97.
[45] S.W.S. McKeever, A review of the optically and thermally stimulated luminescence properties of aluminosilicates, Opt. Mater. X 24 (2024) 100351.
[46] V. Correcher, J.M. Gomez-Ros, J. Garcia-Guinea, Radiation effect on the 400-nm-thermoluminescence emission of a potassium-rich feldspar, Radiat. Meas. 38 (2004) 689–693.